NANO LETTERS

Letter

pubs.acs.org/NanoLett

Label-Free Segmentation of Co-cultured Cells on a Nanotopographical Gradient

Paul M. Reynolds,[†] Rasmus H. Pedersen,[†] John Stormonth-Darling,[†] Matthew J. Dalby,[‡] Mathis O. Riehle,[‡] and Nikolaj Gadegaard*,[†]

[†]Division of Biomedical Engineering, School of Engineering, University of Glasgow, Glasgow, G12 8LT, United Kingdom

[‡]Center for Cell Engineering, Institute of Molecular Cell and Systems Biology, University of Glasgow, Glasgow, G12 8QQ, United Kingdom

S *Supporting Information*

ABSTRACT: The function and fate of cells is influenced by many different factors, one of which is surface topography of the support culture substrate. Systematic studies of nanotopography and cell response have typically been limited to single cell types and a small set of topographical variations. Here, we show a radical expansion of experimental throughput using automated detection, measurement, and classification of co-cultured cells on a nanopillar array where feature height changes continuously from planar to 250 nm over 9 mm. Individual cells are identified and characterized by more than 200 descriptors, which are used to construct a set of rules for label-free segmentation into individual cell types. Using this approach we can achieve label-free segmentation with 84% confidence across large image data sets and suggest optimized surface parameters for nanostructuring of implant devices such as vascular stents.

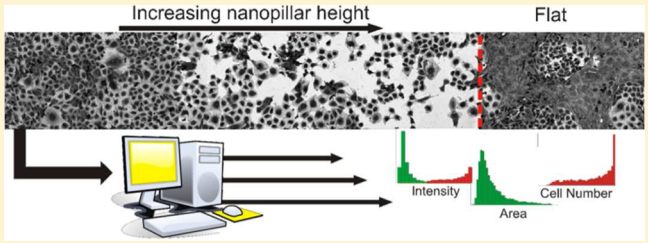

KEYWORDS: *Nanotopography, co-culture, machine learning, high-throughput screening, label free*

It has been reported that there are more than 400 distinct cell types that make up the adult *Homo sapiens* body with functional tissue rarely existing as a homogeneous population of cells.[1,2] With this in mind, it is of critical importance that when screening novel biomedical materials,[3] topographies,[4] and drug targets[5] in vitro, researchers have the ability to utilize heterogeneous populations of cells and so develop real biological context.[6,7]

Cell type specific antibody staining, for example, using banks of cluster of differentiation (CD) markers, is the most predominant method used currently for segmentation after cell culture experiments. However labeling individual cell types imposes a burden of cost and time, and with increasing stringency increasing numbers of experimental repeats, while also limiting the flexibility to costain for other cellular responses such as metabolomic activity[8] and stem cell differentiation.[9] Alternatively, cells may be preloaded with tracker probes for live tracking of cells in co-culture; however, the retention time of these dyes limits experiments to approximately 100 h. In addition, the small molecule tracker dyes may also have an undetermined impact on cellular processes, perhaps influencing the cellular response itself. Cell type segmentation has also been demonstrated by preloading of quantum dots to assess cell adhesion across micropatterned gradient substrates.[10] However, these techniques require isolation of each cell type for particle loading which represents a major problem in the study of diverse primary cultures. Manual segmentation by visual inspection is possible to an extent, Figure 1, although as data sets increase in size this becomes a significant limitation to experimental throughput and the bias of the individual undertaking the analysis becomes increasingly problematic.

Rapid micrograph analysis and machine learning techniques are now accessible with relative ease at the bench research level thanks to the open source CellProfiler[11] and CellProfiler Analyst[12] software suites, respectively, with other tools also available.[13,14] This represents an opportunity to apply automated image analysis to the generation of large empirical data sets from microscopy data, where previous analyses were predominantly subjective. Jones et al. demonstrated the use of such data sets to train a machine learning algorithm to detect 15 varied morphological changes in RNA interference screens.[15] We propose that this method can be applied to the label free segmentation of co-cultures, allowing more detailed analysis of in vitro models of in vivo systems.

Alongside the need to expand cell culture experiments to heterogeneous cell populations, there is also a need to increase the number of parameters screened on a single substrate to mitigate errors introduced by intersample variation and increased experimental processing. This expansion of motifs contained on a single sample may take the form of arrayed surface features,[4,16,17] or alternatively a continuous gradient in

Received: November 6, 2012
Revised: December 17, 2012
Published: December 20, 2012

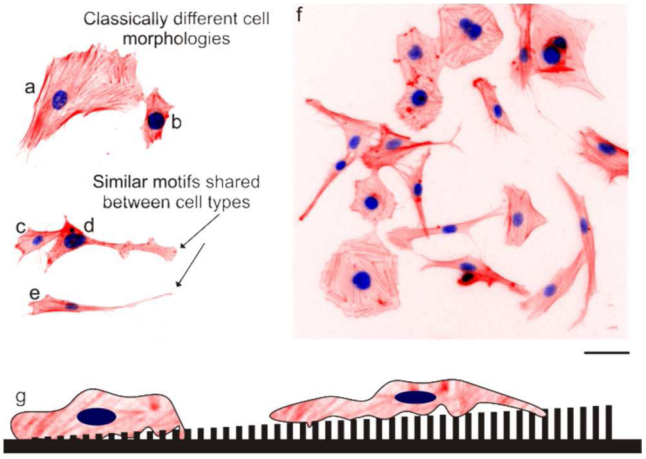

Figure 1. Challenges associated with manual segmentation of co-cultures arise from the diversity of phenotypes on display across a single cell type. On a flat surface, fibroblasts a and e can display drastically different morphologies. Endothelial cells b, c, and d also display a broad variation in appearance. In this instance, only the difference in the structure of uropodia (arrows) indicates that d and e are different cell types. Manual classification of large numbers of images containing many cells, such as image f, is therefore both time-consuming and prone to a level of subjective error. Illustration g outlines the concept of gradient platforms for screening cellular response to a wider range of topographical motifs. Isolating subtle variations in cell response at different points of a gradient of nanopillar height may provide insight into the optimal pillar dimensions. Cell cytoskeleton is labeled with rhodamine phalloidin (red) and nuclear DNA is labeled with DAPI (blue). Scale bar: 50 μm.

which features are varied over a millimeter or centimeter scale.[18,19] Surface gradients of chemistry[20−22] and topography[18,23] have been demonstrated, along with a combination of the two.[24] We present a novel method for fabrication and mass replication of substrates with a continuous gradient of feature height, in this case nanopillars. This method can be readily applicable to any lithographically predefined two-dimensional pattern. On this nanopillar gradient topography, Figure 1g, we demonstrate a technique for the rapid and efficient segmentation of diverse cell populations without the need for extra labeling steps, by processing cell morphology and cytoskeletal structure with machine learning algorithms. The relative response, morphological characteristics, and abundance of each cell type may then be related to the underlying topography at that point, and this insight applied to the design of future tissue engineering constructs such as cardiovascular stents.[25]

To satisfy the need for high-volume, high-fidelity replication of nanostructured cell culture substrates, we show replication of a nanostructured master by injection molding of polystyrene (PS). Injection molding, used for decades in industrial manufacture of parts on the millimeter-scale and above, has in recent years been shown to be capable of replication on the nanometer-scale, for both academic[26−29] and industrial applications (e.g., Blu-ray Discs).

The particular nanostructure used in this work is a regular array of nanoscale pillars, a topography that is known to influence the adhesion, proliferation, and differentiation of a range of cell types.[9,30] Notably, we have previously shown that regular nanopillar arrays can have a cell selective influence on different cell types. Arrays of 110 nm tall pillars were shown to enhance endothelial attachment and proliferation, while inhibiting fibroblast proliferation, when cultured separately on polycaprolactone (PCL).[31] It is known that the depth or height of patterns have significant influence on cell adhesion[32] and thus producing a sample with a continuous variation in height over a long distance (1 cm or more) will allow for rapid investigation of optimal parameters for substrate driven cell separation. In addition, a simple and effective method of co-culture analysis allows the effect of nanotopographical stimulation on the two cell types to be confirmed in a more realistic representation of the in vivo environment.

Briefly, fabrication begins with a clean quartz substrate (25 mm × 25 mm × 1 mm) coated with a 110 nm layer of PMMA (Elvacite 2041, Lucite International). A 20 nm layer of aluminum is evaporated on the sample for charge compensation during electron beam exposure. A 9 × 9 mm^2 regular dot array (100 nm diameter dots on a 300 nm pitch) is defined by single-pixel exposure[33] using a Vistec VB6 UHR EWF system. The total exposure time is approximately 1.5 h. After development in 1:3 MIBK/IPA, 40 nm of aluminum is evaporated on the surface and the structure is lifted off in hot (50 °C) Microposit remover 1165 (Shipley), Figure 2a.

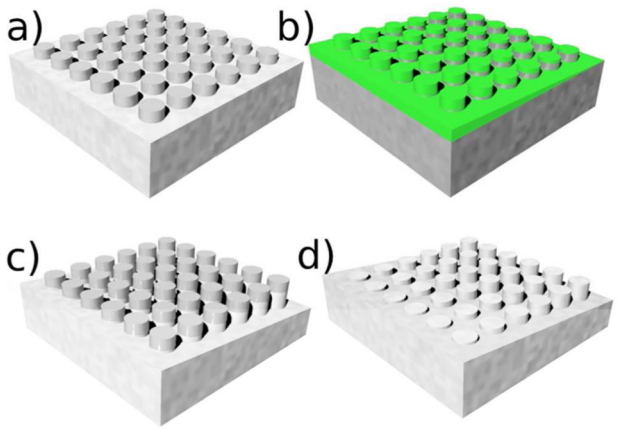

Figure 2. Fabrication flow of topographical gradient structures (not to scale). (a) An array of aluminum nanodots is defined on the substrate using electron beam lithography and lift-off. (b) ppHex is deposited through a mask opening resulting in a thickness gradient across the 9 mm pattern. (c) After plasma etching using the ppHex as a sacrificial layer, the gradient is transferred to the substrate. Pattern dimensions remain defined by the unetched aluminum. (d) The aluminum layer is removed by wet etching, finalizing the master. The master is replicated in PS by injection molding as described in the main text.

To define a smooth variation (gradient) in the eventual pattern height, the sample is coated with a thin layer of plasma polymerized hexane (ppHex), Figure 2b. Further details of the ppHex deposition process have been published elsewhere.[20,34,35] The nanopattern defined in aluminum and the superimposed gradient defined in ppHex are transferred to the substrate using standard RIE processes for quartz: CHF_3/Ar (Oxford Instruments 80+ RIE)). The etch is timed to stop shortly after all the plasma polymer material has been etched Figure 2c. After etching, the aluminum is removed by wet etching, revealing an array of pillars with a variation in height across the sample Figure 2d.

Mass replication of the gradient pattern is carried out by injection molding, Figure 3, for which an inlay is created from the quartz substrate as described previously.[29] The quartz master is gently pressed into contact with a 50 μm layer of SU-

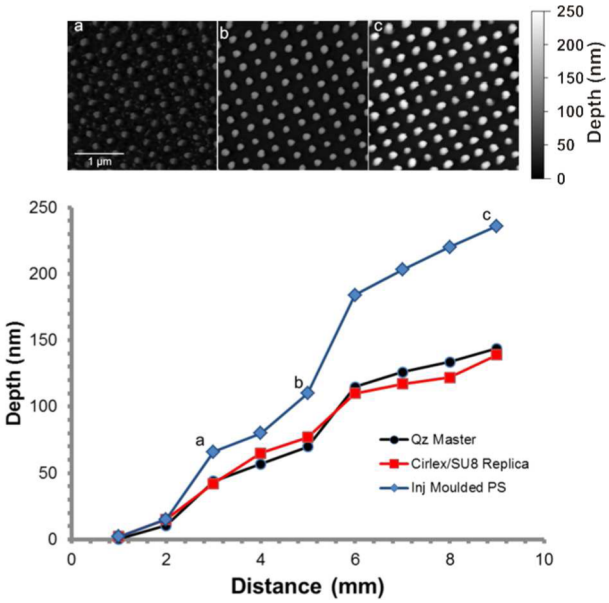

Figure 3. Depth profile of quartz master, injection molding inlay replica, and the final molded part in polystyrene, accompanied by selected AFM scans of features at the shallow (a), medium (b), and tall (c) region of the injection molded sample. A stretching effect is observed in pillar height, as the low thermal conductivity of the polyimide inlay results in the polystyrene being at or near its glass transition temperature at the point of ejection from the molder as reported previously.[29] This gives a further enhancement in the gradient of pillar height.

8 3050 (microChem) on a 770 μm thick polyimide substrate (Cirlex, Katco Ltd.) at a temperature of 96 °C. The SU-8 is exposed for 4 min after which the stack is cooled and separated. The Cirlex piece with patterned SU-8 layer is used directly as an inlay for injection molding. PS replicas were manufactured in an injection molding system (Victory 28, Engel GmbH) and produced samples with a high fidelity to the master in lateral dimensions with an increase in pillar height due to a stretching effect which has been previously observed. Further details of the SU-8 replication and injection molding processes are published elsewhere.[29]

PS replicas of the gradient pattern were prepared for cell culture by 30s treatment in a 30W air plasma, followed by sterilization by immersion for 10 min in 70% ethanol and thorough rinse in sterilized, deionized water before being allowed to air dry overnight in a sterile environment. PS was chosen for injection molding samples due to its excellent replication of nanofeatures[27] and its near ubiquitous use in tissue culture. Monocultures and 50:50 co-cultures were seeded on three material replicates, using fibroblast (hTERT-BJ1) and endothelial (LE2) cells at a density of 5000 cells cm^{-2}. Cell culture media formulations used are included in the Supporting Information. The co-culture suspension was thoroughly homogenized before seeding and care was taken to distribute cells evenly across the topography to prevent localized increases in cell density.

Before combining the two cell populations, the endothelial cells were incubated in suspension with 5 μM green CellTracker dye (Molecular Probes, U.K.) added to the media for 30 min at 37 °C as per manufacturers specifications. Additional washing steps were added to ensure complete removal of excess tracker molecules from the cell suspension. This membrane permeable nonfluorescent dye is taken up by the cells and cleaved by common cellular processes, becoming a cell-impermeable fluorescent tracker. The intensity of endothelial tracker dye reduced with proliferation and there was some uptake of tracker dye by fibroblasts, presumably due to membrane−membrane contact and blebbing during mitosis and cell locomotion.[36] Across the full data set the mean intensity of tracker dye was 5 times higher in LE2 cells versus hTERT cells after 96 h, allowing a robust determination of cell type (a histogram of tracker dye intensity across the data set is provided in the Supporting Information Figure S1). Positive controls confirmed that the dye remained 97% accurate in labeling the endothelial cells after 96 h. Retention of the CellTracker dye after fixation allows straightforward identification of the endothelial subpopulation in fluorescent image sets.

After seeding, the cells were allowed to settle and attach before being moved to an incubator set at 37 °C in a 5% CO_2 atmosphere. Fresh media was added to culture dishes daily, and total culture time was 96 h. After this culture period, cells were fixed in 10% (w/v) formaldehyde solution at 37 °C for 10 min, followed by permeabilization at room temperature for 5 min and nonspecific blocking in 1% (w/v) PBS/BSA for 10 min. F-actin fibers and DNA were stained using phalloidin-rhodamine (Life Technologies) and Vectashield DAPI mounting fluid respectively.

Images of the cultured samples were acquired as a linear scan of 18 contiguous locations across the gradient topography: 4 on the flat substrate, 10 across the pillar gradient, and a further 4 on the flat substrate (Supporting Information Figure S2). Three fluorescent channels were automatically captured for processing using an Olympus CX41 upright microscope equipped with a Prior motorized stage and 10× objective, camera acquisition, and stage were operated by ImageProPlus (Media Cybernetics, UK). A total of 216 locations were captured, comprising 12 linear scans across 3 substrates, Figure 4a. These Images were analyzed using CellProfiler to detect individual cells using the DNA and cytoskeleton stain, Figure 4b. The intensity of CellTracker staining was also measured to act as a positive control classification of the full data set into fibroblast and endothelial cells against which to compare machine learning classification based on the nucleus and cytoskeleton alone.

Processing of the full data set took approximately 2 h on an Intel Core i7 2600 CPU @ 2.4 GHz with 16Gb DDR2 RAM. Over 10 000 individual cells were detected, 200 distinct measurements for each cell computed, and a complete data set contained over 2 million measurements comprising information on cell size, shape, cytoskeletal texture, intensity and location relative to other cells. The data were then transferred into CellProfiler Analyst to initialize training of the machine learning algorithm based classifier to distinguish the two cell types based solely on "cytoprofile" measurements.

Using the CellProfiler Analyst classifier tool, 400 randomly selected cells were sorted by visual inspection of tracker dye intensity as fibroblasts or endothelia, as described by Jones et al.[15] Images of both cell types in monoculture were also used to similar effect. This training set was used to generate a set of rules for segmentation of the images using the tracker probe information, focusing on a threshold intensity of the tracker dye within the detected cell shape, as was anticipated, to determine cell type. The full data set was classified using these rules with 20 random images selected (approximately 800 cells) and inspected with no visible mis-classifications, Figure 4c. To

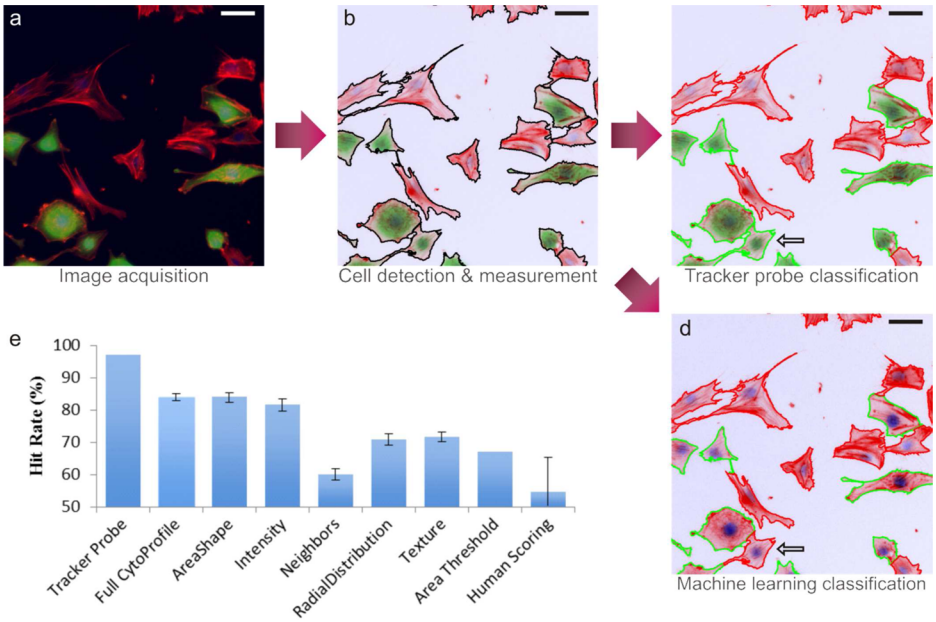

Figure 4. Process flow and accuracy for detection of cell types within a co-culture. (a) Immunofluorescence images are captured of co-cultured cells on nanopillar substrates; nuclear DNA (DAPI, blue) and cytoskeleton (phalloidin−rhodamine, red) are labeled with fluorescent markers. Before the cultures were combined, one cell type (LE2 endothelial) was loaded with a CellTracker dye (FITC, green). (b) The CellProfiler software suite is used to batch process 216 image sets, measuring 200 distinct attributes of 10 237 individual cells. The CellProfiler Analyst classifier can then be used to classify each cell as belonging to either the endothelial class or the fibroblast class. (c) Using the tracker probe intensity to segment images into endothelial (green outline) and fibroblast (red outline) yields an accuracy of 97%. (d) An accuracy of 83.9% can be achieved using only the cytoskeleton stain, i.e., shape, staining intensity, texture, radial distribution, and cell neighbors. (e) Changing the feature sets available to the machine learning algorithm in creating classification rules has an impact on accuracy, offering insight into the dominant features that enable correct classification. A simple filter which divides the co-culture by a cell area threshold is less than 70% accurate, Supporting Information Figure S3. The arrow in panels c and d indicates an endothelial cell that is correctly classified using CellTracker information; however, it is mistakenly classified as a fibroblast using cell phenotype based machine learning classification. Scale bar: 50 μm, error bars represent where possible as standard deviation of individual scans across gradient topography.

determine the experimental error that may be induced by poor retention of the tracker dye, monocultures were processed under the same conditions. The labeling dye stability was assessed by a monoculture of endothelial cells loaded with the fluorescent tracker for 96 h and segmentation of these monocultures using the co-culture segmentation rules. An accuracy of 97% after 96 h culture, Figure 4e, indicated minimal levels of mis-classification due to poor dye uptake by the endothelial cells or poor retention due to loss of cytoplasm/blebbing.

Segmentation of the co-culture using only DNA and cytoskeleton images was carried out by removing the CellTracker information from the data set, Figure 4d. The training set that had been created previously was used, ensuring that cells presented to the algorithm as endothelial or fibroblast were correctly identified. This generated a set of 50 rules (Supporting Information data S5) to classify cells based on morphology (i.e., aspect ratio, area, perimeter, nucleus size) and also the organization of the cytoskeleton (i.e., radial distribution of actin intensity, actin texture). These rules differentiate between the two cell classes by means of the GentleBoosting algorithm, wherein each rule is a regression stump[37] relating to a measured attribute. Visual observation of the cells did indeed indicate that size and cytoskeletal organization are valid methods of distinguishing between the two, and a human may draw on these factors. However, when human classification is compared to rules generated by a machine learning algorithm it is clearly impractical for a human to consider 50 rules when classifying each cell; reinforcing the power of this new methodology.

Classification of the full 10 000 cell data set using the same rules gave an accuracy of 83.9%, Figure 4e. This is shown alongside the accuracy achieved by omitting various other measurement classes from the learning algorithm. This indicates the relative importance of certain feature sets in cell classification and can provide insight into the characteristic differences between the two cell types from a computational standpoint. Accuracy for each cell type was consistently lower for endothelial cells compared to fibroblasts (Supporting Information Figure S4). As a comparison, a simple filter, which sets a threshold of cell size, based on the relative distribution of sizes within each population (MG63 cells Figure S3) has an accuracy of 67%. To indicate the efficacy of this technique, a group of 20 researchers of varied experience and specialty were asked to classify images of 50 randomly selected cells after a brief training session on the characteristics of each cell type. The highest individual score was an accuracy of 70%, while the average score was comparable to randomly classifying each cell with an accuracy of 52%.

With a view to understanding the scalability of this method toward co-cultures of more than a single pair of cell types, a set of 15 images containing 468 MG63 cells (a human osteosarcoma cell line) was introduced into the data set alongside the co-culture images. The classifier was modified to include a third classification bin for the new cell type, which was populated with 100 randomly selected MG63 cells. On the basis of this new training set of three distinct cell types, 50 rules

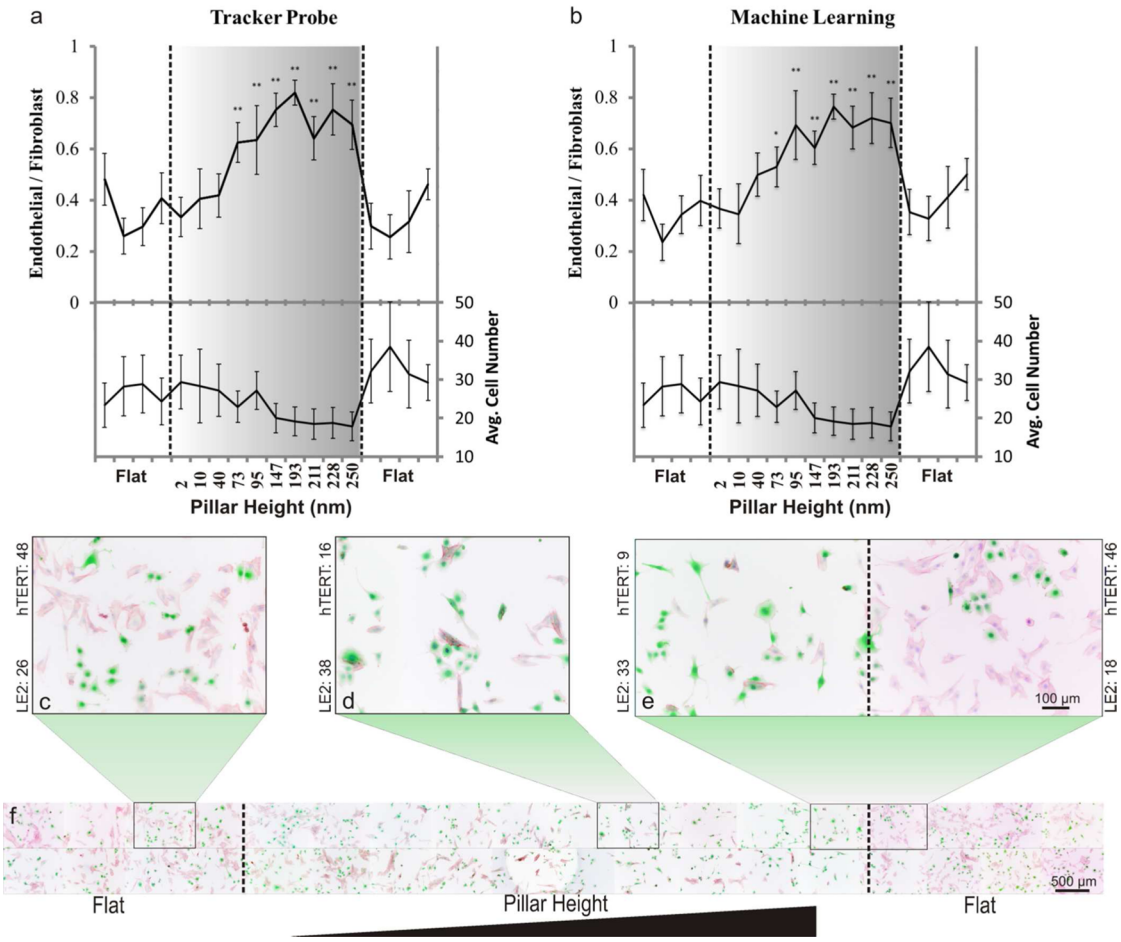

Figure 5. Response of fibroblast (hTERT-BJ1) and endothelial (LE2) cells in co-culture to a gradient of nanopillar height is shown. The ratio of endothelial/fibroblast cells after 96 h culture was calculated by (a) direct labeling of the subpopulations with CellTracker probes and (b) applying machine learning to cell morphology and nucleus data to predict cell type; greyscale background gradient represents increasing pillar height from left to right with dashed line indicating the nanopillar-flat boundary. Statistically, each data point was compared to the "baseline" flat region, $*p < 0.01$, $**p < 0.001$. Images (c−e) show cellular response at various points across the nanogradient sample (f). From this analysis, we can suggest that a nanopillar height in excess of 75 nm is sufficient to induce a statistically significant change in the ratio of endothelial/fibroblast cells on the nanopattern, however as pillar height increases the average number of cells per frame was found to fall.

were once again generated to classify both the co-culture images and also the MG63 cell images. MG63 cells (94.2%) were classified correctly with 4.9% misclassified as endothelial cells and the remaining 0.9% misclassified as fibroblasts (Supporting Information Table S6 and Figure S7). The higher propensity to misclassify MG63 cells as LE2 endothelial cells can be attributed to their similarity in terms of cell size and, to some extent, shape. Further expansion to more complex co-cultures will be strongly dependent on the cell types themselves having suitably distinct features.

This new methodology for the rapid screening and analysis of co-cultures was applied to screening co-culture response across the high throughput nanopillar gradient topography, ranging from a planar surface to a regular array of 250 nm high pillars. This continuous variation of feature height across a substrate provides a modulated stimulation, whose effect on cellular response can be extrapolated from the extensive measurements collected by CellProfiler. Having shown previously that regular nanopillar arrays can exert a cell specific effect on proliferation and adhesion,[31] this gradient topography was devised as a means of finding the "optimal" pillar height for enhanced endothelial response in a co-culture environment under substrate driven cell separation.

After initial seeding of the two cell types at an even density across the nanotopographical gradient, the ratio of endothelial to fibroblast cells varied over time as a function of the underlying and local topographical motifs. Cells were fixed after 96 h culture, resulting in a final distribution of cells which was a combination of proliferation and migration − which have both been shown to be influenced by nanotopographical stimulation. The number of fibroblasts was found to fall steadily with increasing nanopillar height, while there was a moderate increase in the abundance of endothelial cells with increasing pillar height, although endothelial cell numbers also fell away at extreme pillar heights.

There was no evidence that cells were capable of sensing the local gradient of pillar height as the gradient was shallow, rising from a planar surface to 250 nm high pillars across a 9 mm pattern. The average major axis length of endothelial and fibroblast cells was 54.9 and 72.8 μm, respectively, giving a nominal local gradient in pillar height of 1.53 and 2.02 nm across individual cells. Local gradients of approximately 2 nm allow cell activity at any point across the gradient to be

considered as a response to a single pillar height. This allows a high-resolution determination of the impact of varied pillar heights up to 250 nm on cell shape and structure.

Comparison of the ratio of endothelial to fibroblast cells as pillar height increases suggests that there is a height at which the cell selective response of the topography is "switched on" and a statistically significant change in the ratio is observed. At the same time, a reduction in the total cell number is also observed as pillar height increases, Figure 5a,b. This apparent reduction in cell affinity toward tall nanopillars leads to a conclusion that to maximize cell number with the lowest possible ratio of endothelial/fibroblast cells, a pillar height of approximately 75 nm is recommended. This is a promising result, which may be practically applied to the design of cell culture dishes to reduce fibroblast contamination in primary endothelial cultures, and to attempt to prevent restenosis of cardiovascular stents, where the potential of the nano-topography to expedite in situ enothelialization may offer considerable benefits in terms of implant success.

We have compared the ratio of co-cultured cells across a nanopillar gradient by both fluorescent tracker and machine learning classifier analysis. In the data set of 10 237 cells, 1653 cells were misclassified. This amounts to a success rate of 83.9% in the classification of co-cultures by machine learning algorithm, which may be open to improvement through further optimization. Analysis of cell response to the variation in nanopillar height by fluorescent tracker, Figure 5a, or machine learning, Figure 5b, yield the same interpretation of the data in terms of optimal pillar height, indicating that automatic cell type segmentation of co-culture images by machine learning is a viable alternative to fluorescent tracking or antibody staining. Applying this simple and rapid co-culture segmentation technique to gradient and arrayed surface features or chemistries can allow the screening of potential solutions in a context that is closer to the target in vivo system. We propose an optimized pillar height of 75 nm for a targeted increase in the ratio of endothelial to fibroblast cells in co-culture, which may be applied to the future design of cardiovascular implants where rapid enothelialization is required.

■ ASSOCIATED CONTENT

Supporting Information

Description of CellTracker labeling accuracy; data acquisition scheme; fibroblast and endothelial cell size distribution; individual classification accuracy across data set for fibroblast and endothelial cells, and formulations of cell culture media used. This material is available free of charge via the Internet at http://pubs.acs.org.

■ AUTHOR INFORMATION

Corresponding Author

*E-mail: Nikolaj.Gadegaard@glasgow.ac.uk.

Notes

The authors declare no competing financial interest.

■ ACKNOWLEDGMENTS

We would like to thank the staff and technicians of the James Watt Nanofabrication Centre for their assistance during the substrate fabrication process. We would also like to thank the members of the Centre for Cell Engineering particularly Carol-Anne Smith for their help and discussion on the topic of cell culture studies. The work has been partially funded by the Engineering and Physical Sciences Research Council (EPSRC), Grant EP/F500424/1 DTC in Cell and Proteomic Technologies, the Glasgow Research Partnership in engineering (GRPe), and the EC-funded project NAPANIL (Contract no. FP7-CP-IP214249-2). Finally, we would like to thank the creators of CellProfiler for their prompt and informative responses to queries on the CellProfiler Forum (www.cellprofiler.org).

■ REFERENCES

(1) Alberts, B.; Johnson, A.; Lewis, J.; Raff, M.; Roberts, K.; Walter, P. *Mol. Biol. Cell* **2008**, 1725.
(2) Vickaryous, M. K.; Hall, B. K. *Biol. Rev. Cambridge Philos. Soc.* **2006**, *81*, 425−55.
(3) Anderson, D. G.; Levenberg, S.; Langer, R. *Nat. Biotechnol.* **2004**, *22*, 863−6.
(4) Unadkat, H. V; Hulsman, M.; Cornelissen, K.; Papenburg, B. J.; Truckenmüller, R. K.; Post, G. F.; Uetz, M.; Reinders, M. J. T.; Stamatialis, D.; Van Blitterswijk, C. a; De Boer, J. *Proc. Natl. Acad. Sci. U. S. A.* **2011**, *108*, 16565−70.
(5) Geysen, H. M.; Schoenen, F.; Wagner, D.; Wagner, R. *Nat. Rev. Drug Discovery* **2003**, *2*, 222−30.
(6) Kirkpatrick, C. J.; Fuchs, S.; Unger, R. E. *Adv. Drug Delivery Rev.* **2011**, *63*, 291−9.
(7) Khetani, S. R.; Bhatia, S. N. *Nat. Biotechnol.* **2008**, *26*, 120−6.
(8) Ngo, J. T.; Champion, J. a; Mahdavi, A.; Tanrikulu, I. C.; Beatty, K. E.; Connor, R. E.; Yoo, T. H.; Dieterich, D. C.; Schuman, E. M.; Tirrell, D. a *Nat. Chem. Biol.* **2009**, *5*, 715−7.
(9) Dalby, M. J.; Gadegaard, N.; Tare, R.; Andar, A.; Riehle, M. O.; Herzyk, P.; Wilkinson, C. D. W.; Oreffo, R. O. C. *Nat. Mater.* **2007**, *6*, 997−1003.
(10) Rivera Gil, P.; Yang, F.; Thomas, H.; Li, L.; Terfort, A.; Parak, W. J. *Nano Today* **2011**, *6*, 20−27.
(11) Kamentsky, L.; Jones, T. R.; Fraser, A.; Bray, M.-A.; Logan, D. J.; Madden, K. L.; Ljosa, V.; Rueden, C.; Eliceiri, K. W.; Carpenter, A. E. *Bioinformatics* **2011**, *27*, 1179−80.
(12) Jones, T. R.; Carpenter, A. E.; Lamprecht, M. R.; Moffat, J.; Silver, S. J.; Grenier, J. K.; Castoreno, A. B.; Eggert, U. S.; Root, D. E.; Golland, P.; Sabatini, D. M. *Proc. Natl. Acad. Sci. U.S.A.* **2009**, *106*, 1826−31.
(13) Cardona, A.; Tomancak, P. *Nat. Methods* **2012**, *9*, 661−5.
(14) Cho, B. H.; Cao-Berg, I.; Bakal, J. A.; Murphy, R. F. *Nat. Methods* **2012**, *9*, 633−4.
(15) Jones, T. R.; Carpenter, A. E.; Lamprecht, M. R.; Moffat, J.; Silver, S. J.; Grenier, J. K.; Castoreno, A. B.; Eggert, U. S.; Root, D. E.; Golland, P.; Sabatini, D. M. *Proc. Natl. Acad. Sci. U.S.A.* **2009**, *106*, 1826−31.
(16) Anderson, D. G.; Putnam, D.; Lavik, E. B.; Mahmood, T. a; Langer, R. *Biomaterials* **2005**, *26*, 4892−7.
(17) Kolind, K.; Dolatshahi-Pirouz, A.; Lovmand, J.; Pedersen, F. S.; Foss, M.; Besenbacher, F. *Biomaterials* **2010**, *31*, 9182−91.
(18) Kunzler, T. P.; Drobek, T.; Schuler, M.; Spencer, N. D. *Biomaterials* **2007**, *28*, 2175−82.
(19) Gallant, N. D.; Lavery, K. a.; Amis, E. J.; Becker, M. L. *Adv. Mater.* **2007**, *19*, 965−969.
(20) Zelzer, M.; Majani, R.; Bradley, J. W.; Rose, F. R. a J.; Davies, M. C.; Alexander, M. R. *Biomaterials* **2008**, *29*, 172−84.
(21) Simon, C. G.; Lin-Gibson, S. *Adv. Mater.* **2011**, *23*, 369−87.
(22) Glassford, S.; Chan, K. L. A.; Byrne, B.; Kazarian, S. G. *Langmuir* **2012**, *28*, 3174−9.
(23) Ding, Y.; Sun, J.; Ro, H. W.; Wang, Z.; Zhou, J.; Lin, N. J.; Cicerone, M. T.; Soles, C. L.; Lin-Gibson, S. *Adv. Mater.* **2011**, *23*, 421−5.
(24) Yang, J.; Rose, F. R. a. J.; Gadegaard, N.; Alexander, M. R. *Adv. Mater.* **2009**, *21*, 300−304.
(25) De Mel, A.; Jell, G.; Stevens, M. M.; Seifalian, A. M. *Biomacromolecules* **2008**, *9*, 2969−79.

(26) Bakker, R. M.; Boltasseva, A.; Liu, Z.; Pedersen, R. H.; Gresillon, S.; Kildishev, A. V; Drachev, V. P.; Shalaev, V. M. *Opt. Express* **2007**, *15*, 13682−13688.
(27) Gadegaard, N.; Mosler, S.; Larsen, N. B. *Macromol. Mater. Eng.* **2003**, *288*, 76−83.
(28) Schift, H.; David, C.; Gobrecht, J.; D' Amore, a.; Simoneta, D.; Kaiser, W.; Gabriel, M. *J. Vac. Sci. Technol., B* **2000**, *18*, 3564.
(29) Stormonth-Darling, J. M.; Gadegaard, N. *Macromol. Mater. Eng.* **2012**, *297*, 1075−1080.
(30) Curtis, A. S. G. *Eur. Cell Mater.* **2004**, *8*, 27−36.
(31) Csaderova, L.; Martines, E.; Seunarine, K.; Gadegaard, N.; Wilkinson, C. D. W.; Riehle, M. O. *Small* **2010**, *6*, 2755−2761.
(32) Dalby, M. J.; Giannaras, D.; Riehle, M. O.; Gadegaard, N.; Affrossman, S.; Curtis, A. S. G. *Biomaterials* **2004**, *25*, 77−83.
(33) Gadegaard, N.; Thoms, S.; Macintyre, D. S.; Mcghee, K.; Gallagher, J.; Casey, B.; Wilkinson, C. D. W. *Micro* **2003**, *68*, 162−168.
(34) Pedersen, R. H.; Hamzah, M.; Thoms, S.; Roach, P.; Alexander, M. R.; Gadegaard, N. *Microelectron. Eng.* **2010**, *87*, 1112−1114.
(35) Reynolds, P. M.; Pedersen, R. H.; Riehle, M. O.; Gadegaard, N. *Small* **2012**, *8*, 2541−2547.
(36) Boss, J. *Exp. Cell Res.* **1954**, *7*, 215−231.
(37) Friedman, J.; Hastie, T.; Tibshirani, R.; Friedman, B. Y. J.; Hastie, T. 2000, *28*, 337−374.